

RESEARCH ARTICLE OPEN ACCESS

Development and Kinetic Modeling of Continuous-Flow Asymmetric Hydrogenation With Integrated Catalyst Recycling

 Maurice Moll¹ | Thorsten Röder¹  | Björn Wängler² | Carmen Wängler³ | Alexander Fabricius¹ | Nico Maier¹

¹Institute of Chemical Process Engineering Mannheim, Mannheim Technical University of Applied Sciences, Mannheim, Germany | ²Clinic of Radiology and Nuclear Medicine, Molecular Imaging and Radiochemistry, Medical Faculty Mannheim, University Heidelberg, Mannheim, Germany | ³Clinic of Radiology and Nuclear Medicine, Biomedical Chemistry, Medical Faculty Mannheim, University Heidelberg, Mannheim, Germany

Correspondence: Thorsten Röder (t.roeder@hs-mannheim.de)

Received: 27 October 2025 | **Revised:** 14 January 2026 | **Accepted:** 4 February 2026

Keywords: asymmetric hydrogenation | continuous flow | kinetic modeling | process development | scale-up

ABSTRACT

In the development of economic competitive and sustainable pharmaceutical manufacturing with homogeneous catalysts, catalyst recovery is a key step toward efficient and scalable processes, as it directly impacts process efficiency and economic feasibility. In this study, we demonstrate the integration of organic solvent nanofiltration (OSN) into a continuous asymmetric hydrogenation of benzylphenylephrone (BPE) to enable catalyst recycling and process intensification. This is coupled with kinetic modeling for *in silico* investigation of the established process. Membrane screening identified PuraMem Flux as the most suitable material, achieving >90% catalyst retention under operating conditions. Catalyst recycling experiments revealed a reproducible activity loss of ~10% per cycle, which was incorporated into the mathematical model and validated in recirculation operation. Scale-up to a 59.4 mL tubular reactor with an integrated unit for OSN confirmed the accuracy of the model and demonstrated stable operation with consistently high enantiomeric excess (87%–90% ee). Comparative evaluation of single-pass and recirculation operation highlighted the benefits of catalyst recycling, with yields increased from 69.1% to 86.8%, while space–time yield (STY) improved by over 20%. Together, these findings establish continuous asymmetric hydrogenation with catalyst recycling via OSN as a promising route, providing a robust foundation for efficient and sustainable pharmaceutical manufacturing.

1 | Introduction

Hydrogenations are a cornerstone of pharmaceutical synthesis, with approximately 25% of all approved drugs relying on at least one hydrogenation step in their manufacturing [1]. Among these, asymmetric hydrogenation has emerged as an especially powerful method for the creation of enantiomerically pure pharmaceutical intermediates and drug substances, owing

to the high selectivity achievable with suitable homogeneous catalysts [2]. However, the high cost of such catalysts, alongside with product isolation and catalyst separation issues, continues to be a key challenge in industrial synthesis, making catalyst economy an ongoing focus of innovation. Traditional hydrogenations are often performed in multi-purpose batch reactors, where standard vessel volumes of ~1 m³ typically limit safe operating pressures to around 10 bar without costly specialized

Abbreviations: *a*(t), catalyst activity; API, active pharmaceutical ingredient; BPE, benzylphenylephrone; BPR, back pressure regulator; E, extinction; ee, enantiomeric excess; ESI, electronic supplementary; *k_d*, deactivation constant; *m_p*, mass flow; MeOH, methanol; OSN, organic solvent nanofiltration; *p*, pressure; PFA, perfluoroalkoxy alkane; PS, presaturation; *Q_l*, volumetric liquid flow; *R*, universal gas constant; *R*, retention; *R₀*, initial reaction rate; *S/C*, substrate to catalyst ratio; STY, space–time yield; *T*, temperature; *V_R*, reactor volume; *λ*, wavelength; *τ*, residence time.

This is an open access article under the terms of the [Creative Commons Attribution](https://creativecommons.org/licenses/by/4.0/) License, which permits use, distribution and reproduction in any medium, provided the original work is properly cited.

© 2026 The Author(s). *ChemCatChem* published by Wiley-VCH GmbH

equipment [3]. To reduce expenses, these processes are usually carried out with low catalyst loadings under moderate reaction conditions, resulting in long reaction times of several hours, ultimately impacting process economics [4, 5]. Continuous flow processing offers a compelling alternative to conventional batch operation. Their inherent design offers improved environmental, health, and safety profiles, as well as process intensification via higher operational pressures, smaller reaction volumes, and direct integration with downstream separation. These higher working pressures, especially for gas-liquid reactions, increase gas solubility and allow for both higher catalyst turnover frequencies (TOF) and lower catalyst loadings, delivering substantial cost and sustainability benefits [6, 7]. Over the past decade, continuous hydrogenation has matured significantly in pharmaceutical manufacturing, including applications to stereoselective and asymmetric transformations. Recent studies have demonstrated that continuous flow reactors can deliver high conversions and enantioselectivities for asymmetric hydrogenations under intensified conditions, highlighting their potential for scalable and efficient synthesis of active pharmaceutical ingredients (APIs) [8–10].

While continuous asymmetric hydrogenations have been reported in the literature, including recent examples employing modern flow reactor designs and homogeneous rhodium as well as immobilized catalysts [7], their implementation at a process-relevant level remains challenging. Batch processes remain dominant in pharmaceutical practice due to the high flexibility, shortened development times and avoidance of capital investment risks, especially when late-stage clinical results are pending. The resulting reliance on established batch equipment leaves considerable untapped potential for process improvement, such as enhanced efficiency alongside improved environmental, health, and safety profiles, while the inherent equipment design enables operation at substantially higher pressures [3, 11].

This issue is especially highlighted by large-volume commodity APIs such as phenylephrine. Phenylephrine, an α -1 adrenergic agonist, is widely used to treat hypotension, as a nasal decongestant, and in ophthalmology for pupil dilation and vasoconstriction [12, 13]. Structurally closely related to ephedrine, epinephrine and salbutamol, phenylephrine shares pharmacological attributes with these sympathomimetic amines, but its uses and regulatory acceptance make it a globally important API [14]. The pharmaceutical potential makes phenylephrine an ideal model for developing a synthesis process applicable to all related molecules. Recent market analyses estimate the annual global production of phenylephrine hydrochloride at approximately 2000–5000 metric tons [15–17], underlining its significance for both generic and proprietary pharmaceutical manufacturers. On an industrial scale, the well-established synthetic pathway for this pharmaceutical compound is a homogeneously catalyzed asymmetric hydrogenation in a batch autoclave with relatively long reaction times, caused by low pressures and catalyst loadings to reduce investment, raw material, and operating costs. Although there has been previous work on the continuous operation of asymmetric hydrogenations [3, 6–8, 11, 18–21], the practical integration transition into a continuous process for API production has yet to be realized. In particular, catalyst stability, recovery, and long-term operation represent critical bottlenecks for industrial application.

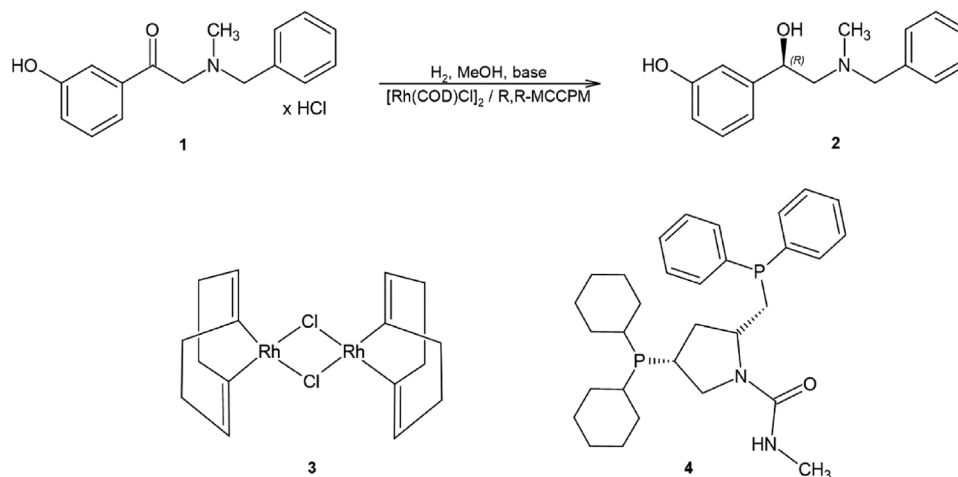
Organic solvent nanofiltration (OSN) has emerged as a promising tool for retaining homogeneous catalysts while allowing low energy selective product removal, and several studies have demonstrated its potential for catalyst recirculation in continuous processes [22–24]. However, OSN performance is highly system-specific and governed not only by molecular weight cut-off but also by solute-membrane interactions, solvent effects, and solution-diffusion transport mechanisms, especially in polar solvents such as methanol [25–27].

In previous work, a continuous lab-scale process of the high-pressure asymmetric hydrogenation of benzylphenylephrine (BPE) to (R)-benzylphenylephrine was developed and optimized. Further, kinetic studies were conducted to create a kinetic model of the reaction [28]. Building on this, this work further investigates the development, including a scale-up of the previously built setup. For this, organic solvent nanofiltration was integrated for efficient catalyst recovery under continuous flow conditions, while catalyst deactivation behavior was systematically evaluated. In addition, the laboratory setup was scaled up and benchmarked against conventional single-pass operation. The combined use of experimental data, kinetic modeling, and process intensification provides a solid foundation for robust, sustainable, and economically viable continuous asymmetric hydrogenations in API manufacturing.

1.1 | Reaction

The underlying reaction in this work is the asymmetric hydrogenation of 2-(benzyl(methyl)amino)-1-(3-hydroxyphenyl) ethanone hydrochloride (or BPE, **1**) to 3-[(1R)-2[benzyl(methyl)amino]-1-hydroxyethyl]phenol (or benzyl-phenylephrine, **2**) in methanol, wherein the benzyl group serves as a protective group (see Scheme 1). 0.1 molar equivalents of diethylamine was used to neutralize the hydrochloride salt. A rhodium-based, in situ formed catalyst was employed, consisting of a catalytically active molecule chloro (1,5-cyclooctadiene, **3**) rhodium(I)dimer([Rh(COD)Cl]₂), and a chiral ligand (2R,4R)-(+)-2-(Diphenylphosphinomethyl)-4-(dicyclohexylphosphino)-N-methyl-1-pyrrolidinecarboxamide (2R,4R-MCCPM, **4**), responsible for imparting enantioselectivity. Notably, Boehringer Ingelheim filed a patent [29, 30] for the industrial asymmetric hydrogenation of phenylephrine in batch mode employing this Rh/COD-phosphine catalyst system, underlining its relevance for scalable pharmaceutical synthesis.

The active catalytic species is proposed to form in situ via initial ligand exchange and cleavage of the dimeric rhodium complex. This is likely leading to a mononuclear Rh(I) coordinated by the chelating diphosphine ligand. Such mononuclear square-planar Rh(I) diphosphine complexes are well documented as catalytically competent in asymmetric hydrogenation of polar substrates, especially in related industrial systems for amino ketone reductions to amino alcohols [5, 31–33]. Literature on related ligand systems suggests that, following H₂ activation and initial hydride transfer, transient intramolecular coordination of the carbonyl oxygen may occur, replacing a coordinated solvent molecule. By this extra coordination, the complex shows increased activity compared to typical Noyori type BINAP catalysts [5, 33]. A possible structure of the active complex with



SCHEME 1 | Asymmetric hydrogenation of 1 BPE to 2 (R)-benzylphenylephrine under use of a rhodium based homogeneous catalyst consisting of the precursor molecules 3 $[\text{Rh}(\text{COD})\text{Cl}]_2$ and 4 2R,4R-MCCPM.

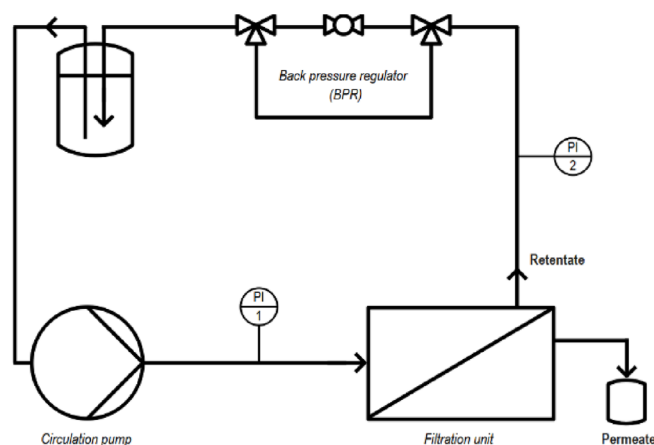
a coordinated substrate molecule was proposed by Klingler [5]. Comparable square-planar Rh(I) diphosphine species with labile ancillary ligands have also been widely discussed in the literature [34, 35].

It is emphasized that this represents one plausible, literature-supported mechanistic scenario. The exact structure, coordination environment, and nuclearity of the active catalyst under the applied reaction conditions remain unproven and were not experimentally resolved within the scope of this study. Based on this tentative structural assignment, the molar mass of the catalytically active species is expected to be higher than that of the individual catalyst precursors and significantly larger than that of the substrate (255.3 g mol^{-1}) and product (257.3 g mol^{-1}). The molecular weight of the active species is thus estimated to exceed 700 g mol^{-1} . Possible dynamic ligand exchange, alternative coordination modes, or different catalytically active species are not excluded and were not further investigated within the scope of this work.

2 | Results and Discussion

2.1 | Organic Solvent Nanofiltration (OSN)

The successful development of the proposed process with catalyst recycling relies fundamentally on selecting an appropriate recycling unit and membrane as well as optimizing process parameters. Therefore, the following section focuses on investigating catalyst recovery using OSN, which, especially in pharmaceutical applications, attracted the attention of industry and academia [36]. Given the significant difference in molecular weights between the catalyst precursors (493.1 and 522.6 g mol^{-1}) and the in situ formed catalytically active complex, which is expected to exhibit an even higher molar mass as explained in the previous chapter, and the comparatively lower molecular weights of the substrate (255.3 g mol^{-1}) and product (257.3 g mol^{-1}), membranes with intermediate molecular weight cut-off (MWCO) values above 300 may, in principle, provide a basis for selective separation. Since the catalyst is intended to remain within the system for recycling purposes, achieving high retention for



SCHEME 2 | Filtration setup with the Evonik MetCell for catalyst recovery via OSN.

the catalyst is crucial. In contrast, the substrate and product should ideally pass through the membrane into the permeate, necessitating low retention for these components.

For the experimental investigation of the feasibility of separating the homogeneous catalyst using nanofiltration, a compact setup was constructed within a laboratory fume hood. The core component of the system is a membrane cell (Metcell, Evonik, Scheme 2), which houses a membrane with an active surface area of 51 cm^2 . The membrane is operated in a crossflow filtration mode, with the solution being pumped across its surface using an HPLC pump (Cole-Parmer High-Flow Dual Piston Pump, VWR). Additionally, the system is equipped with two pressure sensors (HiTec Zang GmbH) to monitor pressure before and after the filtration cell. The connections are made using $1/16''$ and $1/8''$ stainless steel and PFA capillaries. Depending on the experimental conditions, the solution comprises substrate, catalyst, and product dissolved in methanol. The pressure is controlled by a pressure maintaining valve located at the retentate outlet, ensuring consistent pressure throughout the system. The solvent passing through the membrane, referred to as the permeate, is

TABLE 1 | Overview of tested membranes for catalyst recovery with the average fluxes throughout each experiment.

| Company | Name | MWCO | Materials | Flux, avg. ^b (L h ⁻¹ m ⁻²) |
|--------------------|---------------------|-------------------|-------------------------|--|
| Unisol | S-3014 | 400 | Patented composite film | 47.6 |
| Evonik | DuraMem 500 | 500 | P84 polyimide | 50.3 |
| Operations GmbH | PuraMem Selective | n.a. ^a | Silicone-coated PAN | 116.3 |
| | PuraMem Performance | | | 100.1 |
| | PuraMem Flux | | | 118.7 |

^aMWCO is strongly dependent on the solvent and the solute, as molecules solubility dominates membrane separation.

^bAverage fluxes throughout a whole experiment at a recirculation flow rate of 30 mL min⁻¹ and an applied pressure of 20 bar.

collected in a reservoir and exits the system, while the retentate is recirculated.

In total, five different membranes suitable for OSN with methanol were tested, as summarized in Table 1. The solutions used for these experiments included either the substrate, the catalyst, both together, or the product solution obtained from prior reactions carried out in the reactor of the lab-scale process. Samples were collected from both the retentate and the permeate in intervals of 10 or 15 min to measure their concentrations and the amount of permeate. These data were used to determine the permeate volumetric flow rate and, subsequently, the flux. Substrate and product concentrations were analyzed via HPLC and catalyst concentration via UV/vis.

One of the most important parameters for evaluating separation performance is the retention R_i of each component. It can be calculated using the concentrations in the feed $c_{i,feed}$ and the permeate $c_{i,p}$:

$$R_i = 1 - \frac{c_{i,p}}{c_{i,feed}} \quad (1)$$

In addition to retention, the permeate volumetric flow rate and the flux (Table 1) must be considered, as it is a key factor in determining the mass flow of the product leaving the system and, consequently, the overall process productivity. For the comparison of membranes, initial experiments were conducted using only the dissolved substrate. This preliminary screening aimed to identify membranes with the lowest retention of the substrate and product, ensuring their efficient permeation through the membrane. The rationale behind these pretests lies in the high cost of the catalyst and the need to minimize the number of experiments for the initial selection. Membranes that do not exhibit sufficient permeability for the substrate can thus be directly excluded from further investigation. For the experiments, solutions with a concentration of 50 mmol L⁻¹ were prepared and circulated for 120 min. The permeate volume was measured at 15-min intervals, and the substrate concentration in the permeate was analyzed. The permeate concentration profiles are presented in Figure 1a. As indicated by the results, the DuraMem 500 exhibited the poorest performance, with a remarkably low BPE permeability, as evidenced by a high retention of 93.2%, suggesting that this membrane is virtually impermeable to BPE. In contrast, the PuraMem Flux demonstrated the lowest retention at 11.4%, presenting a highly promising perspective for the application of OSN in product separation.

In addition to ensuring sufficiently high substrate permeability, the scalability of the process for potential industrial application requires achieving the highest possible solution flow rate, and consequently, a high mass flow of dissolved BPE. Therefore, in the experiments, the average molar flow rate was determined based on the permeated volume and the measured concentration. For the PuraMem Flux membrane, the average molar flow rate was found to be $\dot{n}_{BPE,avg} = 0.022$ mol h⁻¹ whereas for the PuraMem Selective membrane, the molar flow amounted to only $\dot{n}_{BPE,avg} = 0.012$ mol h⁻¹, although showing similar fluxes. For the Unisol membrane, which exhibited the lowest volumetric permeate flow rate and thus the lowest flux, the resulting molar flow rate reached a maximum of 0.003 mol h⁻¹ owing to the additional pronounced substrate retention. These results clearly underline the inherent trade-off between flux and retention, demonstrating that an optimal balance between the two parameters is crucial for maximizing membrane performance in product separation [37].

In addition to ensuring high permeability for the target product, it is crucial to achieve strong catalyst retention, meaning minimal catalyst permeability, to enable effective separation, recycling, and reuse. To evaluate this under realistic conditions, a catalyst-containing solution was prepared and subsequently subjected to continuous hydrogenation with hydrogen in the laboratory setup. The resulting solution containing under hydrogen, in situ activated species was collected and then introduced into the nanofiltration setup with the PuraMem Flux membrane. The experiments were conducted three times under the same conditions and were analogously performed to those described previously.

As shown in Figure 1b, the spectra of the permeate samples (Samples 1–6), and thus their maximum absorbances at the observed wavelength of $\lambda = 255$ nm, are significantly lower than those of the feed. This clearly indicates that most of the catalyst does not permeate through the membrane. Furthermore, the maximum absorbance at 255 nm $E_{max,255\text{ nm}}$ in the retentate after the experiment was 0.90, compared to 0.74 in the initial feed solution. This suggests a higher concentration of the catalyst in the retentate, which can be attributed to the high retention of the membrane. Through a previously established calibration curve at $E_{max,255\text{ nm}}$, the catalyst concentration was determined, yielding an average retention of 91.3%. These results were finally validated using product solutions from the process, with deviations in substrate and catalyst retention across three experiments amounting to $\pm 2.8\%$.

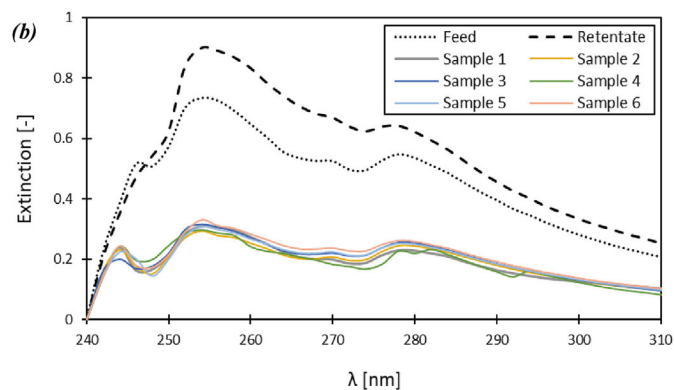
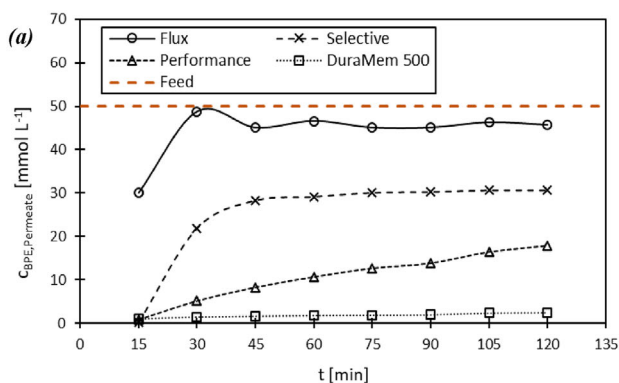


FIGURE 1 | Comparison of substrate concentration in the permeated solution for the tested membranes (left) and spectra of under hydrogen in situ activated species in feed using the PuraMem Flux membrane, retentate and the samples taken during the experiment (right).

While our OSN results demonstrate high catalyst retention and product separation under lab-scale conditions, it is important to position these findings within the broader context of homogeneous catalyst recycling via OSN. For example, Xiao et al. recently reported the application of OSN for the recovery and reuse of a homogeneous palladium catalyst in the pharmaceutical synthesis under industrially relevant conditions, achieving consistent conversion over five reuse cycles [23]. Similarly, technological evaluations by Peddie et al. have shown that OSN can reduce homogeneous catalyst concentrations in the permeate to near negligible levels (< 5 ppm) while offering significant energy and cost savings compared to conventional distillation for post-reaction separations [24]. These examples, together with foundational work by Fassbach et al., underscore the significant progress toward membrane-based recovery of homogeneous catalysts across different reaction types [38]. Comprehensive reviews further highlight that OSN has been extensively explored for the recovery of noble metal catalysts (Pd, Ru, and Rh) and that solvent-membrane compatibility, product purity needs, and catalyst leaching are critical practical considerations for industrial application. In this context, our work complements existing studies by focusing on continuous asymmetric hydrogenation with integrated catalyst recycling and kinetic modeling.

It should be noted that the objective of these experiments was to obtain a rough estimation of the membrane's separation performance, serving as a basis for modeling the system with catalyst recycling. A detailed investigation of membrane-solute affinity, solvent effects, polymer swelling, and non-porous transport mechanisms as well as a mathematical description of these effects on OSN was not intended in this project.

2.2 | Catalyst Deactivation

For the continuous flow experiments for catalyst deactivation evaluation, a setup with a microreactor was used. It consists of a 20 m long coiled 1/16-inch stainless steel capillary with an internal diameter of 1 mm, resulting in a volume of 15.7 mL and is positioned within a temperature-controlled bath thermostat. A detailed illustration of the setup can be found in the [Supporting Information](#). The feedstock was introduced using a continuous syringe pump (SyrDos2, HiTec Zang GmbH, Germany) with 1 mL

high pressure glass syringes. The hydrogen flow was controlled by a digital mass flow controller (EL-FLOW, Bronkhorst High-Tech B.V.). The gas and liquid phases were merged at a T-junction (1.25 mm bore) and then flown through the reactor as a slug flow. Temperature, liquid and gas flow rates were controlled and monitored using a laboratory automation system (HiTec Zang GmbH, Germany). A program was developed within the software to perform these experiments fully automated. This allows different residence times and temperatures to be studied by programmatically adjusting the liquid or gas flow rate and temperature. Downstream of the reactor is a back pressure regulator (BPR, Equilibar, USA) connected to a nitrogen gas cylinder, which allows adjustment and control of the pressure within the system, also monitored by the laboratory automation system. The BPR is followed by an electric valve connected to an automatic sampler (AutoSam, HiTec Zang, Germany) and the product tank. This configuration allows safe, inert and automated sampling. The high operating pressures of up to 65 bar in the test facility make special safety measures essential. Only certified components designed to withstand pressures of at least 90 bar are used, and connections are regularly replaced. In addition, a pressure relief valve is installed upstream of the T-junction, which is activated when the pressure rises to 75 bar, thereby relieving the pressure. As a further measure, the collection vessel is sealed and continuously flushed with argon. This significantly dilutes the remaining hydrogen, which is vented directly into the laboratory fume hood through the connected exhaust pipe, preventing the formation of an explosive atmosphere.

In these experiments, the reaction was conducted in the setup built for performing continuous hydrogenation with a microreactor (see [Supporting Information](#)). Subsequently, the product solution containing the catalyst was used for OSN by passing it through the filtration unit six times. For each pass, the permeate and the retentate were collected and the volumes and the catalyst concentration determined. A new feed solution was then prepared using the collected retentate and filled with solvent and fresh substrate to match the concentrations of the initial feed as closely as possible. The recirculated catalyst solution was then reintroduced into the system to investigate potential activity loss. Experiments were conducted both at constant residence time and with varied residence times to enable a more comprehensive comparison of the activity between the fresh and the recirculated catalyst. Concentration determination was done via HPLC. In the

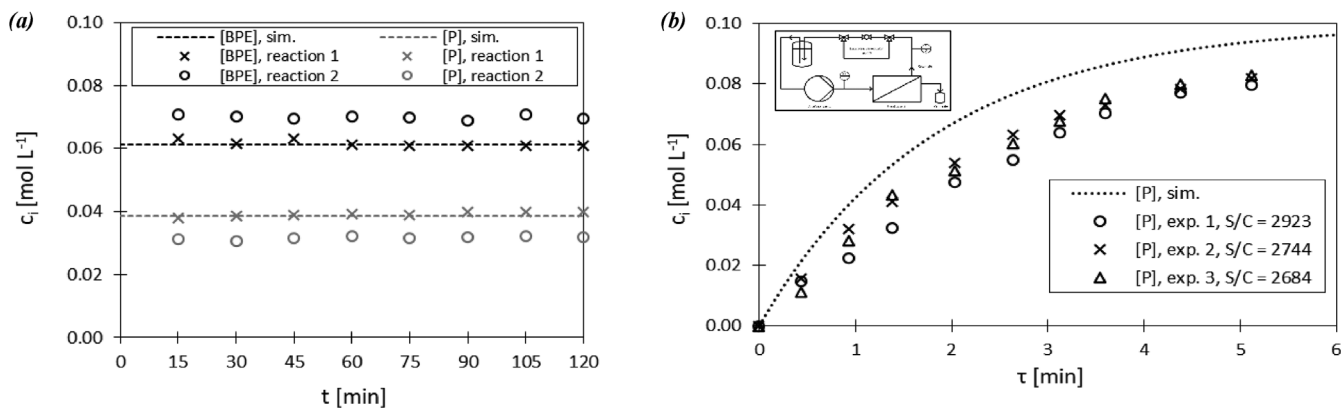


FIGURE 2 | Results of catalyst deactivation experiments at a constant residence time of $\tau = 1.60$ min (a) and varying (b) residence times at $p = 50$ bar, $T = 60^\circ\text{C}$.

following text and figures, the term “product” always refers to the total concentration, including both enantiomers.

Figure 2 presents the concentration profiles of the previously described experiments, while Figure 2a displays the results obtained under constant conditions using the fresh catalyst (reaction 1) and the recovered catalyst (reaction 2). It is evident that in both cases, the concentrations remain highly stable, indicating that no deviations occurred and that the reactions proceeded steadily within the reactor. Furthermore, a clear difference in concentration profiles can be observed: in the second reaction, the product concentration is significantly lower when using the recirculated catalyst, while the concentration of the reactant is higher. This observation clearly indicates catalyst deactivation. The experiment was repeated three times under the same conditions to prove reproducibility. In each case, the measured product concentrations obtained with the recirculated catalyst were approximately 10% lower than those achieved using a fresh catalyst. This decrease was treated as an apparent loss in catalytic performance. It should be noted, however, that this macroscopic decline in activity may originate from multiple effects, including partial catalyst deactivation as well as the potential loss of catalytically active Rh species through membrane permeation in the form of smaller or dissociated complexes. A differentiation between these contributions was not pursued in this study, as the primary objective was to capture the overall performance decay of the integrated process.

Figure 2b illustrates the product concentration profiles from the experiments with the recirculated catalyst at varying residence times compared to the simulated product concentrations obtained with the fresh catalyst. These experiments were also repeated three times, using identical initial concentrations in the first experiment. Due to catalyst recovery via OSN and subsequent replenishment, slight variations in concentration and thus in the substrate-to-catalyst ratio (S/C) occurred in the second reaction. In the simulation, the S/C ratio was set to 2500. Here, too, catalyst deactivation is clearly visible. On average, the loss of catalytic activity is also around 10%, aligning well with the values observed in the other experiments. Moreover, none of the experiments showed a decline in chemical or enantioselectivity.

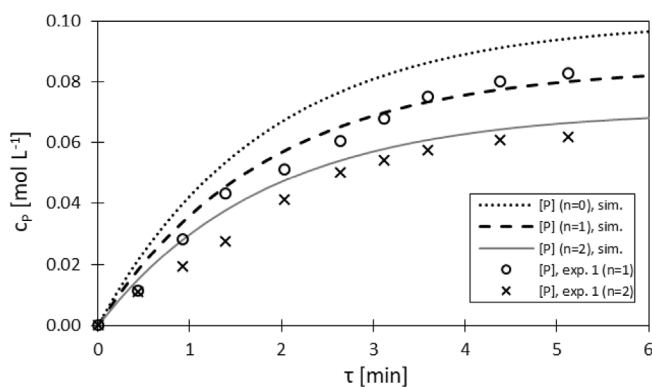


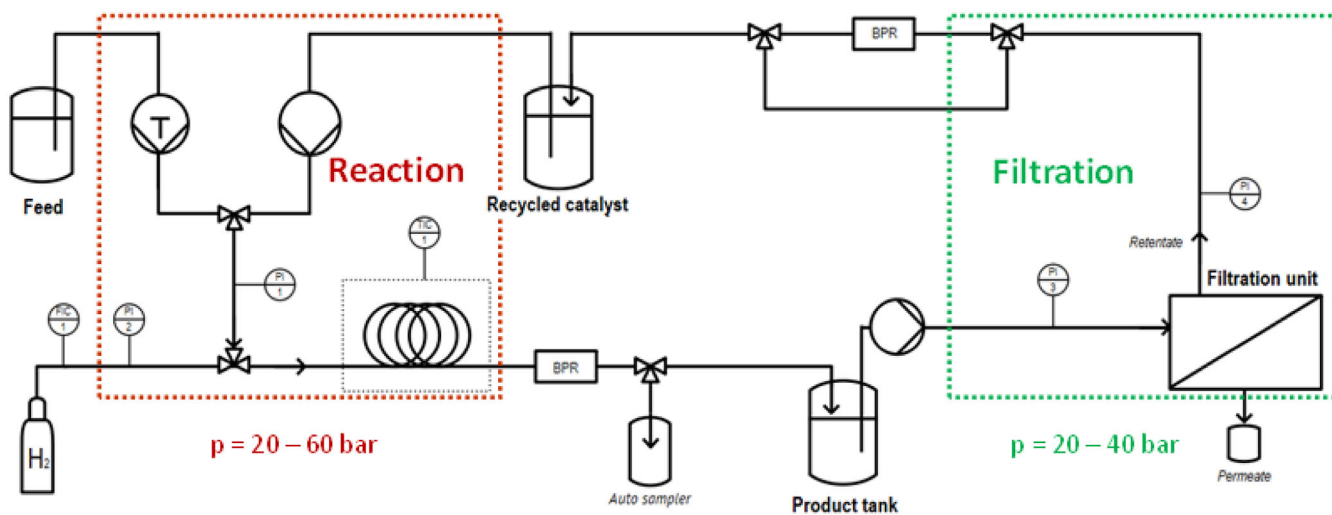
FIGURE 3 | Results of the deactivation experiments over two cycles and comparison with simulated product concentration profiles.

These findings are crucial for a more precise evaluation and modeling of the process with catalyst recycling. To implement catalyst deactivation in our mathematical model for simulating the process, the activity $a(t)$ was defined as an exponentially decreasing function using the deactivation constant k_d :

$$a(t) = e^{-k_d \cdot \left(\frac{t}{\tau}\right)} \quad (2)$$

Since after one cycle, and thus at $\left(\frac{t}{\tau}\right) = 1$, the activity $a(t = \tau)$ is 0.9, the deactivation constant is determined as $k_d = 0.1054 \text{ min}^{-1}$ for the case without the addition of fresh catalyst. It should be noted, however, that it is not entirely certain how and where exactly the catalyst deactivation occurs. Deactivation may take place either during the reaction itself or during the filtration process.

For the commercialization of the process, it is also essential to investigate catalyst deactivation after multiple reuses. In this context, a third series of experiments was carried out in which the same catalyst was reused for a second cycle. The experimental procedure was analogous to that of the previous series. Additionally, the concentration profiles were simulated using Equation (2) and compared with the experimentally obtained values, as shown in Figure 3. It can be clearly shown that the assumptions made for catalyst deactivation are appropriate, as the experimental data were well reproduced using the defined deac-



SCHEME 3 | Scheme of the full lab-scale process with catalyst recovery.

tivation constant. The close alignment between simulation and experiment demonstrates that the implemented model provides a sufficiently accurate description of the deactivation behavior under the investigated conditions. This validates its suitability for integration into the overall process simulation, enabling a more reliable prediction of long-term performance and process efficiency.

2.3 | Lab-Scale Process With Catalyst Recycling

The setup shown in Scheme 3, also referred to as “loop process”, was used to investigate the process with integrated catalyst recycling. It can be broadly divided into a reaction section and a filtration section, which are decoupled from each other. The reaction section is identical to the setup used for the investigation of catalyst deactivation, with the only difference being the addition of a second pump that recirculates the catalyst separated from the product mixture back into the system. The filtration section corresponds to the setup described in the first chapter. The concentrated catalyst is collected in a reservoir connected to the recycling pump. Decoupling these two units offers several advantages: it facilitates a simpler and safer process operation and enables the removal of excess hydrogen from the system by reducing the pressure before the membrane unit. This, in turn, stabilizes the filtration process and minimizes potential adverse effects of dissolved hydrogen on membrane performance.

Here, it is important to ensure that the volumetric flow rates are adjusted so that the flow into the setup matches the flow exiting the system. Since the permeate stream is the only stream leaving the system, the permeate and feed flow rates must be equal. Otherwise, the collection vessel for the product solution would either run dry or overflow. Therefore, the proportion of liquid permeating through and retained by the membrane was determined. This ensured that the feed and permeate flow rates were nearly identical. The flow rate of the recirculated stream was accordingly adjusted to match the retentate stream. The duration of the experiments ranged from five to six hours, ensuring that

the concentrations, and thus the reaction, reach a steady state, allowing for a comparison between the process with catalyst recycling and a conventional single-pass process. Samples were taken at intervals of 5 to 20 min from the product solution, the retentate, and the permeate. Additionally, the mass and volume of the permeate were measured after these time intervals to rule out deviations in the volumetric flow rate.

The results of these experiments were also compared with the simulated results of the model (see [Supporting Information](#) for more information about the kinetic model). In the model, not only reaction kinetics but also various process parameters were incorporated to create a simulation as close to reality as possible. These parameters include the catalyst deactivation rate, a membrane separation factor for the molar flows of dissolved substances, and a partition factor for the volumetric flow in crossflow filtration. The preliminary kinetic investigations the reaction have been reported previously [28].

In Figure 4 the concentration profiles from the simulation are presented, including catalyst and hydrogen concentrations. Figure 4a shows the results of the first conducted experiments compared to the simulated concentrations. Here, a satisfactory agreement with the simulation was already achieved. The initial increase in concentration can be attributed to the initially low reaction rate and the recycling of approximately 17% of both the educt and product. As a result, these two substances accumulate alongside the catalyst. With the rise in catalyst concentration and the corresponding accelerated reaction rate, along with the stabilization of the process, the concentration then slightly decreases again. This trend is also reflected in the simulation. However, a noticeable discrepancy arises when comparing the progression of BPE concentration after reaching the maximum: while the simulated concentration transitions into a steady state after two hours, the actual concentration continuously decreases. This decline was likely caused by membrane fouling due to the precipitation of the educt and/or the catalyst on the membrane surface, leading to a reduction in its concentration in the solvent. This assumption is further supported by mass balance calculations, which revealed a deficit when deposition was not

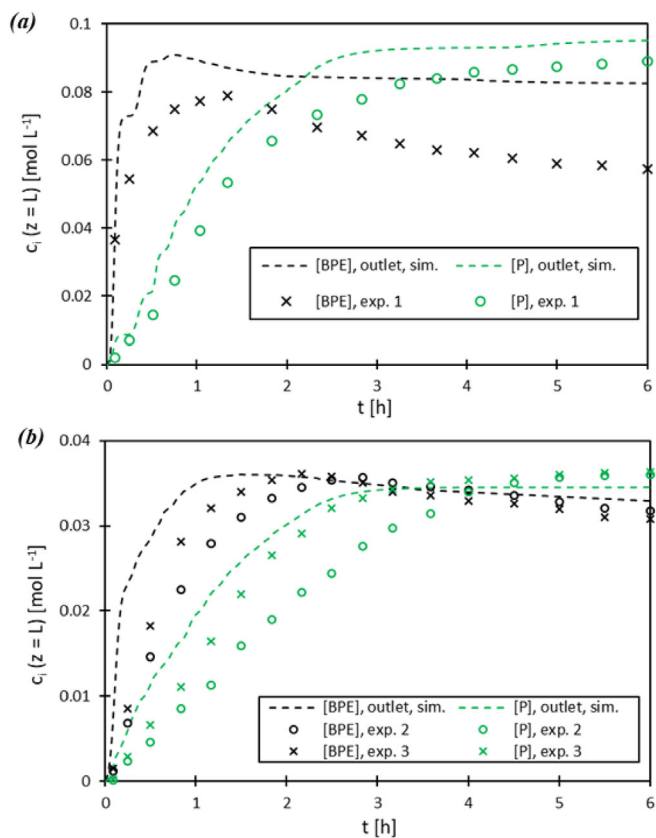


FIGURE 4 | Substrate and product concentrations at time t at the reactor outlet. Conditions: $p = 60$ bar; $T = 80^\circ\text{C}$; $S/C_0 = 7,500$. (a) $[\text{BPE}]_{\text{feed}} = 0.2$ M; $Q_{\text{feed}} = 2.5$ mL min⁻¹; $Q_{\text{recycle}} = 3.5$ mL min⁻¹. (b) $[\text{BPE}]_{\text{feed}} = 0.1$ M; $Q_{\text{feed}} = 3.5$ mL min⁻¹; $Q_{\text{recycle}} = 4.5$ mL min⁻¹.

accounted for, indicating that more material was introduced into the system than has left as permeate.

To reduce membrane fouling caused by precipitation on the membrane surface, the feed concentration was halved from 0.2 to 0.1 M and the volumetric flow rate of the pump feeding the membrane unit was increased from 6.0 to 8.0 mL min⁻¹. Consequently, the fresh feed flow rate was set to 3.5 mL min⁻¹ to match the higher permeate flow and the recirculated stream was set to 4.5 mL min⁻¹. The trend of the simulated concentrations (see Figure 4b) closely resembles those shown in Figure 4a. After reaching a quasi-steady state at approximately 3.5 h of run time, the agreement between the experimental and simulated results improved significantly compared to the initial experiment. After the experiment, the membrane was examined for fouling, revealing significantly less deposition. This finding, along with the improved agreement of concentration profiles, supports the previously assumed hypothesis. In both graphs, particularly the results of exp. 2 in Figure 4b it is noticeable that while the trends are very similar, the measured concentrations are significantly lower than the simulated concentrations, especially during the first three hours. Additionally, the concentration maxima are reached later in reality than in the simulation. These discrepancies could not be eliminated by adjusting the process parameters in the simulation. The simulated process, in contrast to the real process, does not consist of the decoupled unit operations described earlier. Therefore, the real process was further

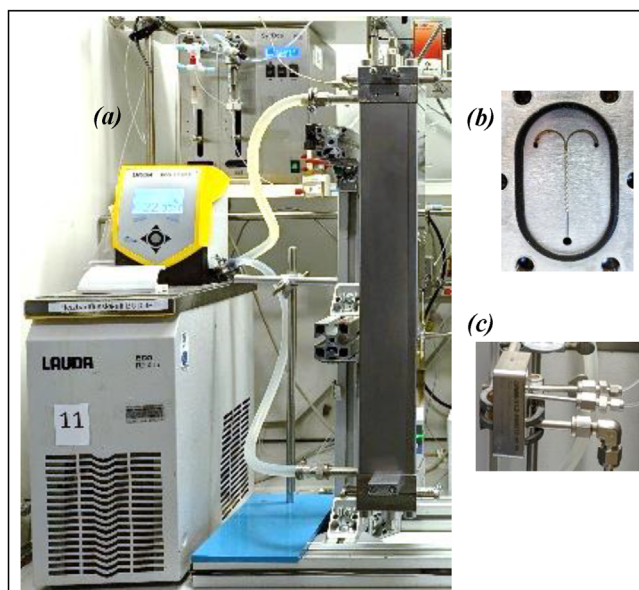


FIGURE 5 | Reactor with thermostat (a); static mixer from the inside (b) and outside (c).

optimized by using smaller collection vessels with a volume of 100 mL instead of 500 mL glass bottles at the reactor and retentate outlets. Furthermore, any residual methanol used to clean the system after previous use and remaining in the setup before the start of the experiment, including in the collection vessels, was replaced with fresh feed solution. The aim was to prevent dilution of the reacting substances and to avoid delays in concentration due to accumulation in the vessels, which had occurred in previous experiments. A significantly improved agreement with the simulation can be seen (Figure 4b, exp. 3), demonstrating that the adjustments led to higher yields and better agreement with the simulated values. Through this stepwise optimization of the setup and its adaptation to the idealized simulation, sufficiently precise predictions of concentration profiles and yields of the lab-scale setup can be made.

2.4 | Model-Based Scale-Up

The most significant modification to the experimental setup for the scale-up experiments was the replacement of the previously used capillary reactor with a double-jacketed tubular reactor from Fluotec Mixing and Reaction Solution AG (Figure 5). This increased the reactor volume from 15.7 to 59.4 mL, resulting in an approximate factor of four, while the inner diameter increased from 1 to 12.3 mm. In addition, the reactor is designed to operate at pressures of up to 60 bar and temperatures of up to 200 °C, thereby enabling the investigation of the same process conditions used in the previous experiments. Due to the twelvefold increase in inner diameter, a static caterpillar mixer for increased mass transfer was installed (600 × 600 μm mixing channels, CPMM R600, Fraunhofer IMM) upstream of the reactor inlet (see Figure 5) to ensure good mixing of the liquid and the gas phase. In the static mixer, hydrogen is introduced into the liquid stream consisting of fresh feed and recirculated stream, where thorough mixing ensures complete dissolution of hydrogen in the solvent. This results in a fully homogeneous phase within the reactor, as

opposed to the previously applied microreactor setup, which operated under a gas–liquid two-phase regime with a high excess in hydrogen. Aside from these modifications, the remainder of the setup remains unchanged and utilizes the same components as described previously. Since the entire system up to the reactor outlet is constructed from stainless steel capillaries, it was not possible to directly observe whether a homogeneous phase was present within the reactor. Although only liquid was observed exiting the reactor, it remained necessary to verify whether any gaseous hydrogen persisted inside the reactor and gradually dissolved into the liquid phase along the reactor length due to the concentration gradient created by hydrogen consumption during the reaction, as the distinction between a fully homogeneous and a two-phase regime directly affects hydrogen availability, reaction kinetics, and mass transfer.

For this purpose, the reaction was first simulated as a single-pass process both with and without hydrogen excess. This results in different reaction rates for both cases due to the varying hydrogen concentrations. While under excess conditions, the dissolved hydrogen concentration can be assumed to be constant and equal to the saturation concentration in the solvent. In the case of no excess, however, the hydrogen concentration decreases over the course of the reaction. The area between these two limiting cases represents an intermediate regime in which hydrogen is present in excess relative to the educt, but its concentration can nevertheless not be assumed to be constant. The effect of the static mixer on productivity was investigated by conducting the experiment with and without the mixer under otherwise identical conditions. In Figure 6, the results of the simulations and the experiments are shown. The results demonstrate that the static mixer significantly influences the conversion rate, particularly at longer residence times and thus lower flow rates. This effect can be attributed to the enhanced mixing efficiency of the two-phase mixture at higher flow rates, where even the T-junction, which is used in the absence of the presaturator, can provide sufficient mixing. However, at lower flow rates, the mixing performance of the T-junction decreases more sharply compared to the static mixer. Moreover, the difference between the two configurations is more pronounced at 40 bar than at 50 bar. This can be explained by the higher hydrogen partial pressure at 50 bar, which results in more hydrogen being dissolved in the solvent even without additional mixing. Nevertheless, conversion remains noticeably higher with hydrogen presaturation through the static mixer. Finally, it can be observed that at shorter residence times, the experimental data align more closely with the simulation assuming hydrogen excess. In contrast, at longer residence times, the experimental values more closely match the simulation without hydrogen excess. One possible explanation lies in the lower conversion at shorter residence times, which leaves a higher excess of hydrogen in the system. Additionally, improved mixing through higher flow rates may enhance hydrogen dissolution. In conclusion, hydrogen presaturation via the static mixer leads to increased productivity in the system.

Finally, the experiments with catalyst recycling were carried out in the same way as previously described to validate the model for scale-up. The experiments were conducted under identical conditions (T , p , flow rates, $c_{\text{BPE},0}$, S/C_0). For the process simulation, the only modification was that the hydrogen concentration was not assumed to be constant, based on the findings from described

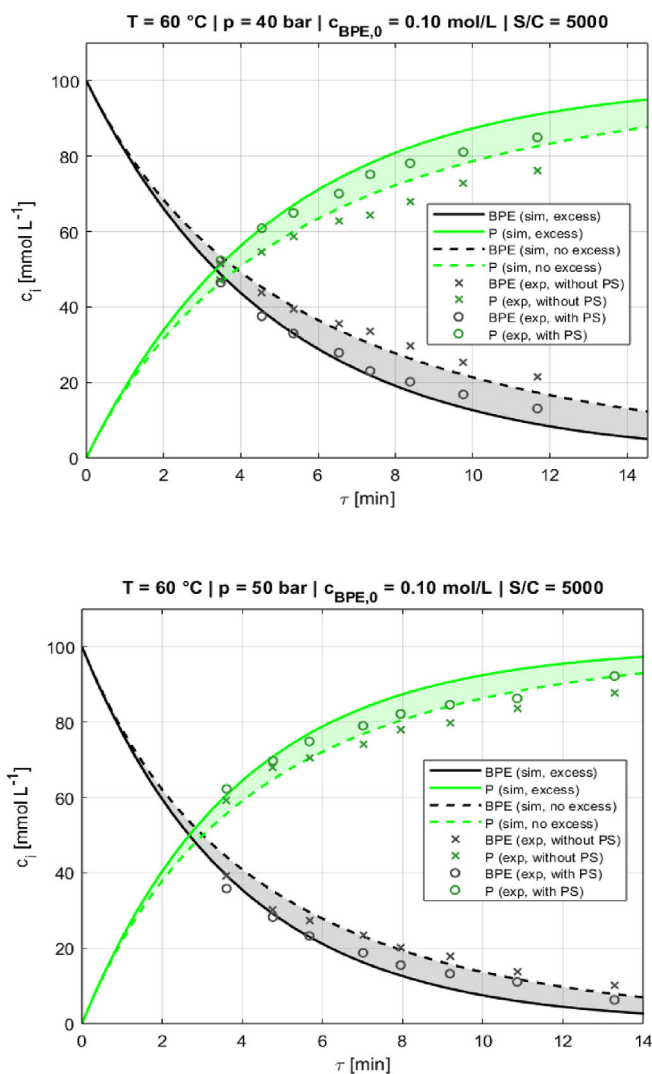


FIGURE 6 | Simulated concentrations with and without hydrogen excess in comparison with and without the use of a static mixer for presaturation (PS). $T = 60^\circ\text{C}$, $p = 40$ bar (top), and 50 bar (bottom).

before. Under these conditions, yields of 86.8% could be observed after reaching steady state. Furthermore, these results verify good hydrogen saturation, as the conversion was high while the hydrogen concentration decreased over the reactor length, which decreased the global reaction rate. The enantiomeric excess remained high (87%–90% ee), confirming that the continuous process preserved chiral integrity. Overall mass balance closure reached approximately 90%, the slight deficit being attributed to minor deposition of the solved substances on the membrane surface, as observed in previous experiments in post-run membrane inspections. As illustrated in Figure 7, concentration profiles measured by HPLC show satisfying agreement with the kinetic model over 300 min, validating its predictive accuracy for extended operation. Simulated and experimental substrate and product concentrations converge closely after 60 min time on stream. Catalyst deactivation behavior in the larger 59.4 mL reactor was, thus, also well described, demonstrating that the deactivation kinetics are reactor-size invariant. Notably, permeate concentrations exceed reactor outlet values by an average of 14% once steady state is reached (Figure 7, right), indicating again an

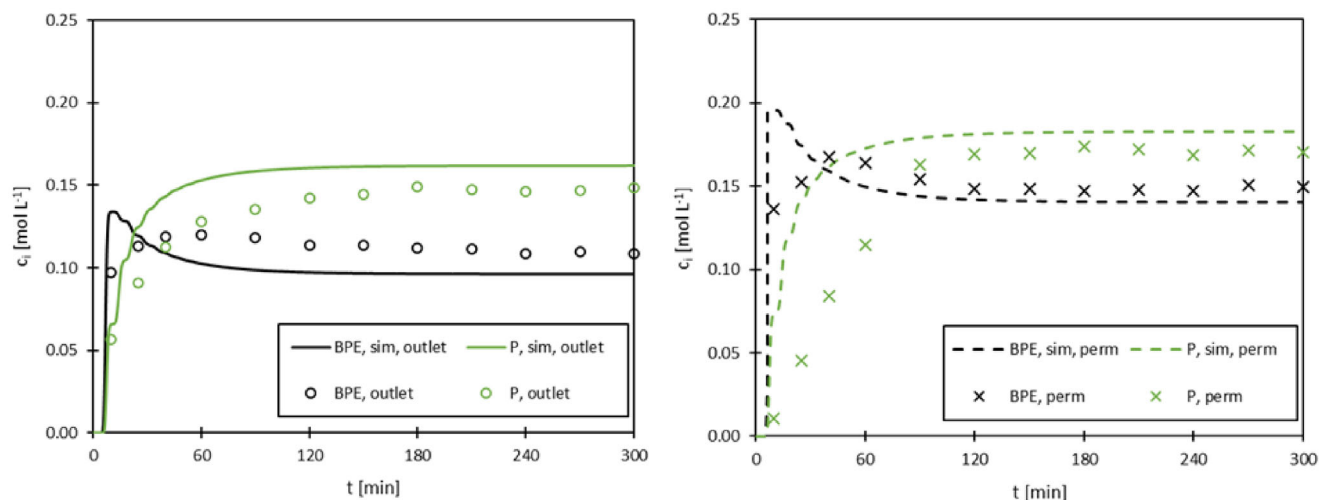


FIGURE 7 | Experimental and simulated concentration profiles of BPE and product. Left: concentrations at the reactor outlet. Right: permeate concentrations.

increase through preferential permeation of both substrate and product through the membrane.

With the validation of the model, the use of this simulation proved particularly advantageous in complementing the experimental work. In addition to capturing start-up dynamics and transient reactor behavior, the model allows for a systematic and efficient exploration of operating conditions without the need for extensive laboratory screening. For example, the influence of the substrate-to-catalyst (*S/C*) ratio could be investigated *in silico*, enabling the identification of an optimal compromise between catalyst cost and product yield. Such model-based studies not only reduce experimental effort and material consumption but also provide valuable insights into the trade-offs between process economics and performance. This simulative optimization thereby establishes a robust framework for rational process intensification and supports the targeted design of scale-up strategies for homogeneous catalytic reactions.

2.4.1 | Comparison of Recirculation, Single-Pass, and Batch Operation

The comparative evaluation of single-pass and loop operation with catalyst recirculation provides clear evidence of the advantages of the recirculation concept for process intensification (Table 2). To ensure comparability, all experiments and simulations were carried out at a fresh feed rate of 2 mL min⁻¹. While the total inlet flow in recirculation operation is higher due to the recirculated stream, only the fresh feed contribution is considered for evaluation. This approach ensures a fair comparison of yields and productivity between operation modes, as it reflects the actual material input to the system. Under otherwise identical conditions, the loop setup with catalyst recirculation (*V* = 59.4 mL, reactor only) clearly outperforms the single-pass configuration. The yield under single pass operation is 69.1% compared to 86.8% achieved with catalyst recycling, while the space-time yield (STY) improves from 82 to 103 kg h⁻¹ m⁻³. The advantage becomes even more apparent when the single-pass setup is adjusted to achieve the same yield. In this case,

the residence time must be more than doubled to 15.6 min, leading to a volumetric feed flow of 0.9 mL min⁻¹, which drastically reduces STY to 46 kg h⁻¹ m⁻³. An alternative way to achieve the same yield in single-pass operation is to increase the catalyst loading. This can be accomplished with a *S/C* ratio of 4450, indicating that more than twice the catalyst amount is required to achieve the same yields as obtained with catalyst recycling. This demonstrates the efficiency of catalyst recycling, as it enables higher yields without compromising throughput at constant fresh feed. When extending the comparison to the entire laboratory setup, including the nanofiltration module (89.6 mL), the yield remains unchanged at 86.8%, while STY decreases to 69 kg h⁻¹ m⁻³. This reduction highlights an important consideration: although reactor-based metrics emphasize the benefits of the loop process, plant-wide evaluations must also account for hold-up volumes in auxiliary units. In the present laboratory setup, the filtration unit was intentionally oversized, which leads to an underestimation of the true productivity potential. For industrial application, appropriately scaled separation modules would minimize this effect, allowing the loop process to fully demonstrate its advantages.

To further contextualize the performance of recirculation operation, simulated batch operation was included in the comparison. Batch simulations were conducted at conditions yielding the same overall conversion as achieved in continuous flow (86.8%). For both scenarios, an additional discharge time of 30 min was added to account for realistic autoclave operation. Space-time yields were calculated based on the total product mass in the reactor at the end of the reaction and the overall batch cycle time. A constant hydrogen concentration was assumed, reflecting continuous hydrogen dosing to maintain constant pressure.

In a first scenario, batch operation was simulated under laboratory-accessible conditions (20 bar) with otherwise identical parameters. Even under these favorable conditions, a reaction time of 19.6 min was required to reach the same yield, resulting in a lower STY of 62 kg h⁻¹ m⁻³ compared to loop operation. This reduction reflects the absence of continuous throughput in batch processing.

TABLE 2 | Comparison of process performance metrics (yield, product mass flow rate, and space–time yield) between loop operation with catalyst recycling and single-pass operation, considering reactor-only and full laboratory unit volumes. Conditions: $c_{\text{BPE},0} = 0.2 \text{ M}$, $T = 60^\circ\text{C}$, and $p = 50 \text{ bar}$.

| Operation mode | System boundary and special adjustments | V (mL) | Q_{in}^{a} (mL min ⁻¹) | τ/t_{R} (min) | c_{p} (mmol L ⁻¹) | S/C (-) | Yield (-) | \dot{m}_{p} (g h ⁻¹) | STY (kg h ⁻¹ m ⁻³) |
|---|--|----------|--|-------------------------------|--|---------------|-----------|---|---|
| Loop process with catalyst recirculation Single pass operation | Reactor only | 59.4 | 2.0 | 7.0 | 173.6 | 10,000 | 86.8% | 6.1 | 103 |
| | Reactor and filtration unit | 89.6 | 2.0 | 10.5 ^b | 173.6 | 10,000 | 86.8% | 6.1 | 69 |
| | Same residence time | 59.4 | 2.0 | 7.0 | 138.1 | 10,000 | 69.1% | 4.9 | 82 |
| | Same yield (adjusted flow) | 59.4 | 0.9 | 15.6 | 173.6 | 10,000 | 86.8% | 2.7 | 46 |
| | Same yield (adjusted S/C) | 59.4 | 2.0 | 7.0 | 173.6 | 4,450 | 86.8% | 2.7 | 103 |
| Batch operation ^c | Same yield and S/C (20 bar) | 59.4 | — | 19.6 + 30^d | 173.6 | 10,000 | 86.8% | 3.7 | 62 ^e |
| | Industrial application (10 bar, $S/C = 50,000$) | 59.4 | — | 195.5 + 30^d | 173.6 | 50,000 | 86.8% | 0.8 | 14 ^e |

^aReferring to fresh feed introduced into the system, not the total volumetric flow entering the reactor.

^bResidence time is calculated based on the total volume of reactor plus filtration unit and not the reactor volume alone.

^cSimulated data adjusted to maximum applicable pressure. No batch experiments were conducted under these exact conditions.

^dAdditional changeover time at lab-scale (e.g., discharging the autoclave).

^eVolume filled with reaction solution. Headspace volume is not included.

In a second, industrially realistic scenario (10 bar, $S/C = 50,000$), the reaction time increased to nearly 200 min, leading to a STY of only 14 kg h⁻¹ m⁻³. This highlights the strong impact of reduced hydrogen pressure and catalyst loading on batch productivity.

Overall, the batch simulations demonstrate that, despite comparable yields, batch operation requires substantially longer reaction times and results in significantly lower productivity than the loop process. This clearly highlights the advantages of continuous operation with catalyst recirculation, particularly under industrially relevant constraints. At the same time, batch processing offers important practical advantages, including the widespread availability of established infrastructure, hardware, and operational know-how in industrial environments. Moreover, batch operation avoids the substantial investment costs associated with the implementation of continuous concepts. From a regulatory perspective, especially under GMP conditions, batch processing can further facilitate traceability and documentation, as each batch can be clearly assigned to defined input materials and processing histories.

From an industrial point of view, the evaluation of productivity is crucial. Assuming continuous operation over 8000 h per year, the current laboratory setup at a feed rate of 2 mL min⁻¹ would correspond to an annual production capacity of approximately 49 kg of product. With further scale-up or numbering-up strategies, annual product quantities in the range of several hundred kilograms could be achieved. This demonstrates that the work presented here provides a solid foundation for the industrial translation of the process. For practical implementation, however, certain aspects need to be addressed. Industrial setups would require larger and multiple filtration units to handle increased flow rates and ensure continuous operation. Membrane fouling, observed already at lab scale, would necessitate regular replacement of filtration modules. A realistic operational strategy would therefore involve alternating units, where part of the filtration

modules remain in operation while others undergo membrane exchange, leading to additional operating costs.

Nevertheless, the loop process offers several key advantages. By recycling the catalyst, significantly lower catalyst consumption is required to achieve higher STYs and yields compared to single-pass operation. Moreover, a large fraction of the catalyst is already successfully retained by the membrane, though for pharmaceutical applications under GMP standards, the residual catalyst concentration in the permeate would need to be reduced further, ideally to only a few ppm. Taken together, these results emphasize that loop operation with catalyst recycling not only provides a marked improvement in yield and efficiency under laboratory conditions but also establishes an important technological basis for future industrial implementation. With optimized reactor and separation design, the concept has the potential to deliver competitive productivity while ensuring sustainable catalyst utilization.

3 | Conclusion

In this study, the continuous asymmetric hydrogenation of benzylphenylephrine with integrated catalyst recovery via organic solvent nanofiltration was systematically investigated and modeled. The developed experimental and modeling framework covered reaction kinetics, catalyst deactivation, and membrane separation performance, enabling a holistic evaluation of the process. Catalyst recycling was demonstrated with consistently high retention (> 90%) and no measurable loss of chemoselectivity or enantioselectivity, while the observed deactivation behavior was successfully captured by an exponential decay function and implemented into the kinetic model. This model was subsequently validated under extended operation and scale-up conditions, reliably predicting concentration-time profiles and confirming its transferability across reactor scales. The integration of catalyst recovery in a loop setup significantly

improved process efficiency compared to single-pass operation. Higher yields, product mass flows, and space-time yields were achieved even when accounting for non-constant hydrogen concentrations and realistic membrane performance. Incorporating the filtration unit into the evaluation reduced space-time yield as expected, given its over-dimensioned scale for this setup, but the experiments highlight the strong potential of loop processes for increasing catalyst utilization and overall productivity.

From an industrial perspective, while the applied flow rates of fresh feed of 2 mL min^{-1} are not directly relevant for large-scale production, they provide a consistent basis for comparing process performance with and without recycling. At this scale, the annual production capacity of the presented setup would reach approximately 49 kg, assuming 8000 h of continuous operation. With further scale-up and/or numbering-up strategies, production of several hundred kilograms per year is technically feasible. For such implementation, larger and multiple filtration units would be required, operated in parallel to allow continuous membrane replacement and mitigate fouling-related downtime. Regular membrane exchange would increase operational costs, but the reduced catalyst demand, improved selectivity, and high retention already achieved provide a strong foundation for industrial application. Furthermore, future work must address the reduction of residual catalyst concentrations to a few ppm and increase the optical purity of the obtained product to above 99% ee to comply with GMP requirements. For this, another possibility might be crystallization [5, 39], which should be addressed in further investigations together with other possible solutions.

Overall, this work establishes a solid basis for transferring continuous asymmetric hydrogenation with integrated OSN-based catalyst recovery toward industrially relevant processes in the pharmaceutical industry by integrating known methodologies. The combination of experimental validation and predictive modeling creates a useful platform for future optimization, scale-up, and design of robust, efficient, and selective continuous manufacturing routes for pharmaceutical intermediates.

4 | Experimental and Analytic Section

4.1 | Solution Preparation

The preparation of the solutions used in all experiments was carried out in an identical manner. First, up to 500 mL of methanol (HPLC grade, $\geq 99.9\%$, Bernd Kraft) was degassed using a degasser, and the storage vessel was purged with argon to displace air and ensure an inert atmosphere. Subsequently, the catalyst (min 98%, Strem Chemicals Inc.), and substrate (95%, abcr GmbH) were weighed in under argon in a glovebag and transferred into the degassed solvent within the inertized vessel. The resulting solution was stirred on a hot plate set to 50°C using a magnetic stirrer for approximately 10 min. Afterward, 10 mol% diethylamine ($\geq 99.5\%$, Sigma-Aldrich) was added, and the solution was stirred for an additional 10 min. Finally, a sample was withdrawn for determination of the substrate concentration.

4.2 | Filtration Experiments

Membranes of appropriate size were cut from A4 flat sheets. Circular pieces were placed into the designated position of the stainless-steel membrane cell, which was then sealed securely using external clamps. Prior to the experiments, membranes were conditioned by flushing with pure methanol for 1 h at ambient temperature to remove potential impurities. Experimental solutions were prepared as described in Section 4.1. The feed solution was introduced into the membrane module at defined flow rates and pressures using an HPLC pump. Permeate and retentate streams were collected separately, and volumetric flow rates were monitored gravimetrically over time. All experiments were conducted at room temperature, 20 bar and a volumetric liquid flow of 30 mL min^{-1} . The concentrations of substrate, product, and catalyst in permeate and retentate samples were analyzed by HPLC and UV/vis, respectively. From these data, solute retention was calculated, with catalyst retention and substrate passage serving as key metrics for membrane performance.

4.3 | Single Pass Experiments

At the beginning of each run, the system was purged with argon. Afterward, methanol and hydrogen flow were started, and the system pressure was slowly increased using nitrogen, supplied from a gas bottle connected to the back-pressure regulator. Once stable operating conditions were reached, the feed solution was switched to the product solution. After two residence times, the experiments were started. For catalyst deactivation experiments at constant residence time, samples were collected every 15 min to monitor the deactivation. For residence time variation experiments, samples were taken after 1.5 residence times to ensure steady-state conditions.

4.4 | Experiments With Catalyst Recycling

The experimental procedure was analogous to the single-pass experiments, with the main difference that the setup was connected to the membrane filtration unit. A second pump was employed to recirculate the catalyst retained in the retentate back to the reactor. Both permeate and retentate samples were collected every 15 min for concentration analysis.

4.5 | Analytical

4.5.1 | HPLC

From each sample, 100 μL was pipetted and diluted with 1 mL of methanol in a vial for HPLC analysis. The chromatographic separation was performed using a chiral Lux 3 μm i-cellulose-5 column ($150 \times 4.6 \text{ mm}$, Phenomenex, Germany). The mobile phase consisted of 85% *n*-hexane, 14.9% ethanol, and 0.1% ethylenediamine and was pumped with 1 mL min^{-1} through the column. This method enables the separation of the two enantiomers formed during the reaction, allowing for the determination of enantiomeric excess (ee).

4.5.2 | UV/Vis

The catalyst concentration was determined using UV/vis spectroscopy (DR 5000, Hach Lange) within a wavelength range of 250–400 nm.

Supporting Information

Further details on the analytical methods employed are provided in the [Supporting Information](#).

Author Contributions

Maurice Moll: investigation, programming, and writing – original draft. Carmen Wängler: supervision – reviewing, editing, and discussion. Björn Wängler: supervision – reviewing, editing, and discussion. Thorsten Röder: funding acquisition, supervision, conception, and writing – reviewing and editing. Alexander Fabricius and Nico Maier: investigation and programming. All authors have given approval to the final version of the manuscript.

Acknowledgments

This work was funded by the German Federal Ministry of Research (BMBF) and EUROAPI Germany GmbH as part of the Innovation Partnership M2Aind Project 13FH8I04IA and 13FH8I11IA within the framework “Starke Fachhochschulen-Impuls für die Region” (FH-Impuls). The authors would like to thank Francois Kruger (EUROAPI Germany GmbH), Norbert Egger (Echnaton Mainz GmbH), and Charles Gordon (Scale-up Systems Ltd.) for great technical support.

Open access funding enabled and organized by Projekt DEAL.

Conflicts of Interest

The authors declare no conflicts of interest.

Data Availability Statement

The data that support the findings of this study are available from the corresponding author upon reasonable request.

References

1. A. Adamo, R. L. Beingessner, M. Behnam, et al., “On-Demand Continuous-Flow Production of Pharmaceuticals in a Compact, Reconfigurable System,” *Science* 352, no. 6281 (2016): 61–67, <https://doi.org/10.1126/science.aaf1337>.
2. J. F. McGarrity and A. Zanotti-Gerosa, “A Feasibility Study on the Synthesis of Phenylephrine via Ruthenium-Catalyzed Homogeneous Asymmetric Hydrogenation,” *Tetrahedron: Asymmetry* 21, no. 20 (2010): 2479–2486, <https://doi.org/10.1016/j.tetasy.2010.09.013>.
3. M. D. Johnson, S. A. May, J. R. Calvin, et al., “Development and Scale-Up of a Continuous, High-Pressure, Asymmetric Hydrogenation Reaction, Workup, and Isolation,” *Organic Process Research & Development* 16, no. 5 (2012): 1017–1038, <https://doi.org/10.1021/op200362h>.
4. T. Ohkuma, D. Ishii, H. Takeno, and R. Noyori, “Asymmetric Hydrogenation of Amino Ketones Using Chiral RuCl₂ (diphosphine)(1,2-diamine) Complexes,” *Journal of the American Chemical Society* 122, no. 27 (2000): 6510–6511, <https://doi.org/10.1021/ja001098k>.
5. F. D. Klingler, “Asymmetric Hydrogenation of Prochiral Amino Ketones to Amino Alcohols for Pharmaceutical Use,” *Accounts of Chemical Research* 40, no. 12 (2007): 1367–1376, <https://doi.org/10.1021/ar700100e>.
6. B. Gutmann, D. Cantillo, and C. O. Kappe, “Continuous-Flow Technology—A Tool for the Safe Manufacturing of Active Pharmaceutical Ingredients,” *Angewandte Chemie International Edition* 54, no. 23 (2015): 6688–6728, <https://doi.org/10.1002/anie.201409318>.
7. G. Farkas, J. Madarász, and J. Bakos, in *Asymmetric Hydrogenation and Transfer Hydrogenation*, Ed: V. Ratovelomanana-Vidal, P. Phansavat. 1st ed. (Wiley, 2021).
8. L. Zheng, W. Feng, C. Chen, et al., “Development of a Heterogeneous P–N–N Tridentate Ligand for Iridium-Catalyzed Asymmetric Hydrogenation of Ketones in Batch and Flow,” *Green Chemistry* 27, no. 14 (2025): 3684–3692, <https://doi.org/10.1039/D5GC00487J>.
9. T. Kuremoto, T. Yasukawa, and S. Kobayashi, “Continuous-Flow Asymmetric Hydrogenation for the Synthesis of an (S)-Metolachlor Intermediate Using Catalysts Immobilized on a Core/Shell-Type Support,” *Advanced Synthesis & Catalysis* 366, no. 4 (2024): 757–761, <https://doi.org/10.1002/adsc.202301251>.
10. D. Geier, P. Schmitz, J. Walkowiak, W. Leitner, and G. Franciò, “Continuous Flow Asymmetric Hydrogenation With Supported Ionic Liquid Phase Catalysts Using Modified CO₂ as the Mobile Phase: From Model Substrate to an Active Pharmaceutical Ingredient,” *ACS Catalysis* 8, no. 4 (2018): 3297–3303, <https://doi.org/10.1021/acscatal.8b00216>.
11. S. A. May, M. D. Johnson, J. Y. Buser, et al., “Development and Manufacturing GMP Scale-Up of a Continuous Ir-Catalyzed Homogeneous Reductive Amination Reaction,” *Organic Process Research & Development* 20, no. 11 (2016): 1870–1898, <https://doi.org/10.1021/acs.oprd.6b00148>.
12. R. R. Ruffolo and J. E. Waddell, “Receptor Interactions of Imidazolines: A-Adrenoceptors of Rat and Rabbit Aortae Differentiated by Relative Potencies, Affinities and Efficacies of Imidazoline Agonists,” *British Journal of Pharmacology* 77, no. 1 (1982): 169–176, <https://doi.org/10.1111/j.1476-5381.1982.tb09283.x>.
13. The Merck Index: An Encyclopedia of Chemicals, Drugs, and Biologicals, *Journal of the American Chemical Society* 129 no. 7 (2007): 2197, <https://doi.org/10.1021/ja069838y>.
14. H. J. Ellner and J. P. Flanagan, “Veno-Ureteric Fistula; a Complication of Aortic Surgery,” *Northwest Medicine* 67, no. 10 (1968): 848–851.
15. Global Phenylephrine Hydrochloride API Market Size And Forecast, Verified Market Research 2025.
16. Phenylephrine Drugs Market Size & Share Report, Global Market Insights 2024.
17. Research and Markets, Phenylephrine Drugs Global Market Report 2025 2025.
18. R. van Putten, N. S. Eyke, L. M. Baumgartner, et al., “Automation and Microfluidics for the Efficient, Fast, and Focused Reaction Development of Asymmetric Hydrogenation Catalysis,” *ChemSusChem* 15, no. 14 (2022): 202200333, <https://doi.org/10.1002/cssc.202200333>.
19. M. T. Ravanchi, *New Advances in Hydrogenation Processes—Fundamentals and Applications* (InTech, 2017), <https://doi.org/10.5772/62820>.
20. Y. Hu, W. Wu, X.-Q. Dong, and X. Zhang, “Efficient Access to Chiral 1,2-Amino Alcohols via Ir/f-Amphox-Catalyzed Asymmetric Hydrogenation of α -Amino Ketones,” *Organic Chemistry Frontiers* 4, no. 8 (2017): 1499–1502, <https://doi.org/10.1039/C7QO00237H>.
21. B. S. Nagy, A. Maestro, M. A. Pericàs, C. O. Kappe, and S. B. Ötvös, “Unlocking the Phosphoric Acid Catalyzed Asymmetric Transfer Hydrogenation of 2-Alkenyl Quinolines for Efficient Flow Synthesis of Hancock Alkaloids,” *Organic Letters* 27, no. 13 (2025): 3414–3419, <https://doi.org/10.1021/acs.orglett.5c00842>.
22. J.-K. Schnoor, J. Bettmer, J. Kamp, M. Wessling, and M. A. Liauw, “Recycling and Separation of Homogeneous Catalyst From Aqueous Multicomponent Mixture by Organic Solvent Nanofiltration,” *Membranes (Basel)* 11 no. 6 (2021): 423, <https://doi.org/10.3390/membranes11060423>.
23. H. Xiao, W. R. F. Goundry, R. Griffiths, Y. Feng, and S. Karlsson, “Recovery and Reuse of Homogeneous Palladium Catalysts via Organic

Solvent Nanofiltration: Application in the Synthesis of AZD4625,” *Green Chemistry* 27, no. 12 (2025): 3186–3196, <https://doi.org/10.1039/D4GC06334A>.

24. W. L. Peddie, J. N. Van Rensburg, H. C. M. Vosloo, and P. Van Der Gryp, “Technological Evaluation of Organic Solvent Nanofiltration for the Recovery of Homogeneous Hydroformylation Catalysts,” *Chemical Engineering Research and Design* 121 (2017): 219–232, <https://doi.org/10.1016/j.cherd.2017.03.015>.

25. J. Shen, K. Beale, I. Amura, and E. A. C. Emanuelsson, “Ligand and Solvent Selection for Enhanced Separation of Palladium Catalysts by Organic Solvent Nanofiltration,” *Frontiers in Chemistry* 8 (2020): 375, <https://doi.org/10.3389/fchem.2020.00375>.

26. H. Ben Soltane, D. Roizard, and E. Favre, “Effect of Pressure on the Swelling and Fluxes of Dense PDMS Membranes in Nanofiltration: An Experimental Study,” *Journal of Membrane Science* 435 (2013): 110–119, <https://doi.org/10.1016/j.memsci.2013.01.053>.

27. V. Masliy, S. M. Guillaume, C. Fischmeister, and J.-F. Carpentier, “Molecular Weight Enlargement of Homogeneous Catalysts for Enhanced Recovery via Organic Solvent Nanofiltration: A Critical Review,” *Coordination Chemistry Reviews* 536 (2025): 216640, <https://doi.org/10.1016/j.ccr.2025.216640>.

28. M. Moll, B. Wängler, C. Wängler, and T. Röder, “Kinetic Investigation of the Asymmetric Hydrogenation of Benzylphenylephrone in Continuous Flow,” *Chimia* 79, no. 6 (2025): 441–448, <https://doi.org/10.2533/chimia.2025.441>.

29. K. F. Dietrich and W. Lienhard, *Verfahren Zur Herstellung von Adrenalin*, EP1210318B1, n.d..

30. K. Paul, A. Lenhart, and F. Dietrich Klingler, *Verfahren Zur Herstellung von (r)-Salbutamol*, EP1585718B1, n.d..

31. R. Noyori and H. Takaya, “BINAP: An Efficient Chiral Element for Asymmetric Catalysis,” *Accounts of Chemical Research* 23, no. 10 (1990): 345–350, <https://doi.org/10.1021/ar00178a005>.

32. R. Noyori, “Asymmetric Catalysis: Science and Opportunities (Nobel Lecture) Copyright© The Nobel Foundation 2002. We Thank the Nobel Foundation, Stockholm, for Permission to Print this Lecture,” *Angewandte Chemie International Edition* 41, no. 12 (2002): 2008, [https://doi.org/10.1002/1522-3773\(20020617\)41:12<2008::AID-ANIE2008>3.0.CO;2-4](https://doi.org/10.1002/1522-3773(20020617)41:12<2008::AID-ANIE2008>3.0.CO;2-4).

33. I. D. Gridnev and T. Imamoto, “On the Mechanism of Stereoselection in Rh-Catalyzed Asymmetric Hydrogenation: A General Approach for Predicting the Sense of Enantioselectivity,” *Accounts of Chemical Research* 37, no. 9 (2004): 633–644, <https://doi.org/10.1021/ar030156e>.

34. J. Daubignard, M. Lutz, R. J. Detz, B. De Bruin, and J. N. H. Reek, “Origin of the Selectivity and Activity in the Rhodium-Catalyzed Asymmetric Hydrogenation Using Supramolecular Ligands,” *ACS Catalysis* 9, no. 8 (2019): 7535–7547, <https://doi.org/10.1021/acscatal.9b01809>.

35. J. Halpern, “Mechanism and Stereoselectivity of Asymmetric Hydrogenation,” *Science* 217, no. 4558 (1982): 401–407, <https://doi.org/10.1126/science.217.4558.401>.

36. H. Xiao, Y. Feng, W. R. F. Goundry, and S. Karlsson, “Organic Solvent Nanofiltration in Pharmaceutical Applications,” *Organic Process Research & Development* 28, no. 4 (2024): 891–923, <https://doi.org/10.1021/acs.oprd.3c00470>.

37. H. B. Park, J. Kamcev, L. M. Robeson, M. Elimelech, and B. D. Freeman, “Maximizing the Right Stuff: The Trade-Off between Membrane Permeability and Selectivity,” *Science* 356, no. 6343 (2017): eaab0530, <https://doi.org/10.1126/science.aab0530>.

38. T. A. Fassbach, J.-M. Ji, A. J. Vorholt, and W. Leitner, “Recycling of Homogeneous Catalysts—Basic Principles, Industrial Practice, and Guidelines for Experiments and Evaluation,” *ACS Catalysis* 14, no. 9 (2024): 7289–7298, <https://doi.org/10.1021/acscatal.4c01006>.

39. A. A. Bredikhin and Z. A. Bredikhina, “Stereoselective Crystallization as a Basis for Single-Enantiomer Drug Production,” *Chemical Engineering*

& *Technology* 40, no. 7 (2017): 1211–1220, <https://doi.org/10.1002/ceat.201600649>.

Supporting Information

Additional supporting information can be found online in the Supporting Information section.

Supporting File 1: cctc70610-sup-0001-SuppMat.docx